IEEE Access
Multidisciplinary | Rapid Review | Open Access Journal

Received September 17, 2020, accepted September 29, 2020, date of publication October 5, 2020, date of current version October 14, 2020.

Digital Object Identifier 10.1109/ACCESS.2020.3028608

A Hybrid Localization Algorithm Based on Doppler Shift and AOA for an Underwater Mobile Node

KUN HAO[1], QIXIN XUE[1], CHENG LI[2], (Senior Member, IEEE), AND KAICHENG YU[1]
[1]School of Computer and Information Engineering, Tianjin Chengjian University, Tianjin 300384, China
[2]Faculty of Engineering and Applied Science, Memorial University of Newfoundland, St. John's, NL A1C 5S7, Canada

Corresponding author: Kun Hao (kunhao@tcu.edu.cn)

This work was supported in part by the National Natural Science Foundation of China under Grant 61902273 and Grant 61962052, in part by the Tianjin Natural Science Fund Project under Grant 18JCYBJC85600, and in part by the Qinghai Key Laboratory of the Internet of Things Project under Grant 2017-ZJ-Y21.

ABSTRACT To solve the problem of low accuracy of a mobile node localization in an underwater sensor network, this article proposes a hybrid localization algorithm based on Doppler shift and angle of arrival (AOA) for the underwater mobile node (DAHL). This algorithm utilizes the Doppler frequency shift between the different signals received from the anchor node and the mobile node and the AOA measurement of the signal reflected by the mobile node to estimate the instantaneous position and velocity information of the mobile node through a two-stage algebraic method. In view of the existing measurement errors in the actual situation, the position and velocity estimation errors of the mobile node are optimized by introducing auxiliary parameters. Theoretical analysis and simulation experiments show that the DAHL method can effectively improve the localization accuracy of the mobile node. The localization accuracy of this algorithm can be close to the Cramér-Rao Lower Bound (CRLB) with the condition of small measurement errors.

INDEX TERMS Underwater sensor network, underwater mobile node localization, Doppler shift, AOA.

I. INTRODUCTION

Underwater sensor networks (UWSNs) are widely used in marine environment monitoring, marine resource development and utilization, geological disaster forecasting, and marine defense security [1]–[3]. Deploying a variable number of sensor nodes with communication capabilities in designated waters is the essential requirement for building the UWSNs. The deployed nodes communicate with each other to achieve collaborative work, and different types of sensor nodes collect various types of data to monitor the underwater environment.

The current communication technologies used by UWSNs primarily include radio waves, optical waves, magnetic induction(MI), and acoustic waves. The transmission distance of the radio signal will be shortened due to the rapid attenuation of radio waves in the water. Background optical pollution, clarity of the water, and optical scattering in the water will have an enormous impact on the communication quality of optical waves, which makes it difficult to transmit over long distances in water with complex diversity. Magnetic induction communication has the characteristics of ensuring transmission rate, low transmission delay [3]. However, the communication range of magnetic induction can only reach 10 to 100 m, which cannot meet the requirements of long distance underwater networking. On the other hand, the attenuation of the acoustic signals in water is small, and the range of acoustic communication can reach several kilometers. Although the acoustic signal has large transmission delay and low data rate, its transmission distance is farther than radio waves, optical waves, and magnetic induction. Therefore, using acoustic waves to communicate becomes the unquestionable choice of UWSNs in recent years.

In UWSNs, underwater node localization has gradually become an indispensable key process. Accurate node location information can help to improve the efficiency of routing protocols, optimize network topology designs, and balance energy consumption in different areas of the network. However, due to the inherent characteristics of underwater acoustic channels, such as high transmission delay, limited bandwidth, Doppler effect, and severe multipath, it has brought great challenges to the localization of UWSNs.

The associate editor coordinating the review of this manuscript and approving it for publication was Emrecan Demirors.

Therefore, the problem of node localization in underwater sensor networks has become a research hotspot in the field of underwater acoustics.

The node localization technologies presently applied to UWSNs mainly include range-based and range-free localization. Range-free localization technologies mainly depend on the connectivity of the network to achieve the position of the node. Besides, the characteristics of link connectivity, signal-to-noise ratio (SNR), and bit error rate (BER) of sensor nodes can also be used. Typical algorithms include centroid algorithm, Approximate Point in Triangle (APIT), and DV-Hop [4]. In the range-based localization technology, the unknown node realizes the estimation of the relative distance and azimuth between itself and the reference node via acoustic signals, and then uses the relevant algorithm to calculate the position [5]. Commonly used measurement methods for range-based localization include time of arrival (TOA) [6], time difference of arrival (TDOA) [7], [8], received signal strength (RSS) [9], angle of arrival (AOA) [10], and combinations of these methods.

At present, localization research on UWSNs is mostly carried out for the localization of nodes in a static environment, many mature algorithms usually relying on different range-based measurement methods, and each measurement method is accompanied by its unique advantages and unavoidable limitations [4], [5]. The TOA-based method uses the signal transmission time and the signal arrival time to determine the one-way distance. This method requires strict time synchronization between the unknown node and the sensor. The TDOA-based method uses the time difference of the signal to reach each sensor node to achieve localization; nevertheless, this method also requires accurate time synchronization between the sensor nodes. The RSS-based method uses transmission loss (power difference between transmitted signal and received signal) as the basis for distance estimation, but in the underwater environment, changes in the underwater acoustic channel will cause the RSS to have a high time-varying characteristic, and it is difficult to accurately measure the signal transmission loss when applying the RSS to underwater localization [11]. AOA-based localization uses the propagation path of the signal to obtain the relative orientation or angle between the node to be localized and the sensor node. On the other hand, during the observation of the target, the underwater sensor node receiving the signal needs to be equipped with a directional antenna with strong directivity to obtain AOA measurements [12]. The method based on AOA measurement requires each sensor node observes the angle of arrival of the signal to generate the coordinates of the target and provide the position information of the node to avoid the ambiguity of localization [13], [14]. To improve the localization accuracy in the underwater environment, multiple measurement methods can be combined to locate the target. Reference [15] proposed a localization method based on bistatic range (BR) and AOA measurements, and the essence of BR is to use ellipse localization. It uses the transmission time of the signal emitted from the transmitting signal sensor and reflected back to the receiving signal sensor via the target. The transmitting signal sensor and the receiving signal sensor are in different positions. This method uses parameter conversion and multistage processing to locate stationary nodes, and its localization accuracy for nodes is high. In [16], the author proposed a hybrid TDOA and AOA method for locating stationary nodes, which has higher localization accuracy than TDOA-based localization alone. The proposed method based on structured total least squares is more robust than the linear least squares method. However, in the actual marine environment, nodes including autonomous underwater vehicles (AUVs), underwater gliders, frogmen, and submarines will move according to application requirements [17]. Because these kinds of nodes have their own velocity, when using the methods for locating stationary nodes to locate mobile nodes, serious errors will arise in the information estimation. The precise localization of underwater mobile nodes is the key to ensuring the completion of various tasks. Consequently, this article has carried out in-depth research on the localization algorithms for underwater mobile nodes.

In the presence of relative motion between the mobile node and the sensor in the UWSN, the impact of the nonnegligible node velocity information on localization performance needs to be fully considered. The localization is far from accurate when only using measurement information such as time difference or angle to locate a mobile node. However, in this case, the signal frequency information is sufficiently accurate, so it can be used to obtain Doppler shift measurements to locate the mobile node. Reference [18] discussed the feasibility of using Doppler shift measurements in underwater localization. The localization accuracy of the target was improved in [19] by combining the spatial correlation of the ocean currents, tracking the speed of sound, using Doppler shift measurements and applying anchor node drift velocity information. Reference [20] proposed a hybrid localization algorithm in a Non-Line-of-Sight (NLOS) environment. This method combines the Doppler shift, TOA, and the angle of departure (AOD) observations, and then uses the least squares technique to estimate the position of the target. However, the application scenario of the method is the localization of moving targets in indoor environment and ground environment with dense buildings. A method for joint localization using Doppler shift and TOA is proposed in [21]. It utilizes information such as the Doppler shift and TOA estimation associated with the moving target node to locate the target, and the combination gives the position and velocity estimation of the moving target. The simulation experiments show that the proposed Doppler-aided method not only improves the position estimation accuracy of the node but also improves the tracking performance.

In summary, when locating an underwater mobile node, a localization method with different measurement parameters is proposed in this article, which can be explored to further improve the accuracy of localization estimation.

The main contributions of the completed work in this article are summarized as follows: (1) this article designs

a network model for mobile node localization in a three-dimensional (3D) underwater scene and combines multiple anchor nodes and ordinary nodes with known positions to locate the mobile node; (2) a hybrid localization algorithm based on Doppler shift and AOA for the underwater mobile node (DAHL), which is suitable for networks operating in nearshore environments, is proposed; (3) similar to the AOA measurements, there are high-dimensional and nonlinear relationships between the Doppler shift and the mobile node localization information, and a two-stage algebraic method is used to linearize these relationships during the localization process; (4) the Cramér-Rao lower bound (CRLB) of the DAHL is analyzed. In addition, through simulation experiments, the superiority and effectiveness of the DAHL algorithm are verified. Naturally, this algorithm will provide a new solution for the localization of the mobile nodes in a 3D UWSN.

The sections in this article are arranged as follows. The network model is established in Section II. Section III introduces the localization model designed on the basis of the network model. In Section IV, a hybrid localization algorithm based on the Doppler shift and AOA for the underwater mobile node is introduced in detail. Section V analyzes the CRLB of the localization algorithm. Section VI presents the experimental simulation results. Finally, the paper is summarized, and the prospective future work is proposed in section VII.

Notations: In the paper, $\boldsymbol{A}^T$ represents the transposed matrix of $\boldsymbol{A}$, $\boldsymbol{A}^{-1}$ represents the inverse matrix of $\boldsymbol{A}$, $\boldsymbol{A}_{p\times q}$ represents a matrix with p rows and q columns, and blkdiag($\boldsymbol{A}$,$\boldsymbol{B}$,$\boldsymbol{C}$) represents the generation of the specified pair where the diagonal elements are the block diagonal matrix of $\boldsymbol{A}$, $\boldsymbol{B}$, and $\boldsymbol{C}$. $\|\cdot\|$ is the Euclidean norm. The operator $\bigotimes$ is a Kronecker product, which represents an operation between two matrices of arbitrary size. For any parameter e, e^0 represents the true value of the parameter e. $\mathbf{0}_q$ represents a q-dimensional zero-column vector. For any vector $\boldsymbol{a}$, it indicates the column vectors, and $\boldsymbol{a}\,(p:q)$ represents the p-th to q-th elements in $\boldsymbol{a}$.

II. NETWORK MODEL

A three-dimensional UWSN is considered and there are M anchor nodes and N ordinary nodes deployed in the UWSN. These nodes are manually deployed in precise positions, and they are connected by cables. Assuming that there is a mobile node $\boldsymbol{u}$ in the UWSN monitoring area, it passes through the network at a certain velocity, and the velocity of the node is much slower than the propagation speed of the communication signal. Multiple anchor nodes equipped with omnidirectional antennas emit monitoring signals of different carrier frequencies, and the monitoring signals are reflected by the mobile node during propagation and received by multiple ordinary nodes. It is assumed that the ordinary nodes know the carrier frequency of the anchor nodes transmitting the monitoring signals, so ordinary nodes can effectively distinguish the received signals of the different types of nodes. Ordinary nodes can obtain the Doppler shift and AOA measurement data from the received signal. Among them, the Doppler shift measurement comes from the frequency difference between the monitoring signal and the reflecting signal received by the ordinary node, and the AOA measurement comes from the angle at which the reflecting signal reaches the ordinary node. The monitoring signal involved in this article refers to the signal transmitted from the anchor node, and the reflecting signal means the signal reflected by the monitoring signal at the mobile node. The AOA refers to the azimuth and elevation at which the reflecting signal reaches the ordinary node. Ordinary nodes send the observed Doppler shift and AOA data information to the shore-based monitoring center through cables, and the monitoring center processes the information to accomplish the localization of the node. The network deployment scenario is shown in Fig. 1.

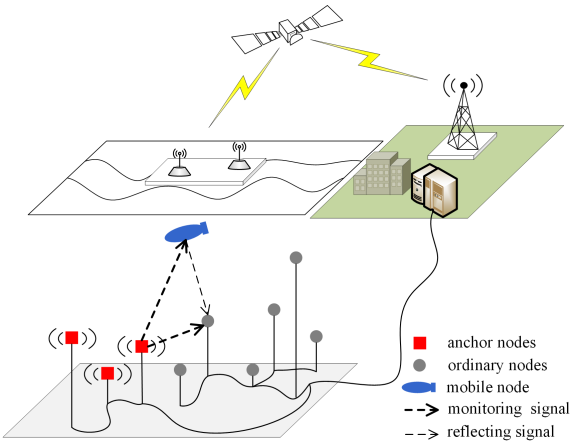

FIGURE 1. Network model. It shows the deployment scenario of the network.

In this scenario, the signals emitted by different anchor nodes do not interfere with each other. Good communication capabilities are maintained between ordinary nodes and the shore-based monitoring center, and all calculations are performed in the same reference system.

III. LOCALIZATION MODEL

The position coordinate of the i-th anchor node in the network is $\boldsymbol{s}_i = [x_i, y_i, z_i]^T$ for $i = 1, 2, \cdots, M$, and the position coordinate of the j-th ordinary node is $\boldsymbol{n}_j = \left[x_j, y_j, z_j\right]^T$ for $j = 1, 2, \cdots, N$. The real position vector of the mobile node is recorded as $\boldsymbol{u}^0 = [x, y, z]^T$, and the real velocity vector is recorded as $\boldsymbol{v}^0 = \left[v_x, v_y, v_z\right]^T$. Every ordinary node in the UWSN can obtain the Doppler shift and AOA measurement. The mobile node localization model is shown in Fig. 2.

In the network, anchor node i transmits a monitoring signal, which is reflected by mobile node $\boldsymbol{u}$, and the frequency at which ordinary node j receives the reflected signal is recorded as [22]

$$f_{i,j} = f_{ci}\left(1 + \frac{v}{c}\left(\cos\theta_{i,v} + \cos\theta_{v,j}\right)\right), \tag{1}$$

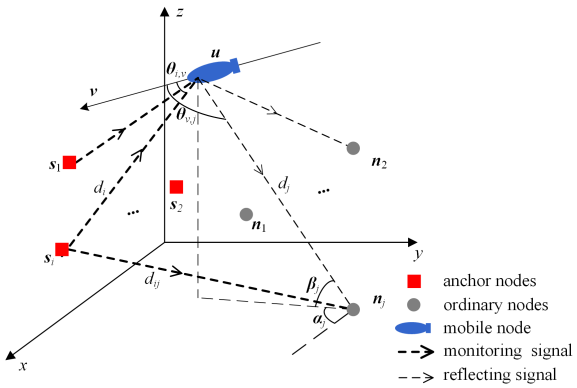

FIGURE 2. Localization model. It shows the localization process of the mobile node.

where $i = 1, 2, \cdots, M, j = 1, 2, \cdots, N, c = 1500$ m/s is the underwater average sound speed, $\theta_{i,v}$ is the angle between the i-th anchor node and the direction of movement of the mobile node, and $\theta_{v,j}$ is the angle between the j-th ordinary node and the direction of movement of the mobile node. Using the cosine theorem, the following can be obtained through (1):

$$f_{i,j} = f_{ci} - \frac{f_{ci}}{c}\left(\psi_i^0 + \psi_j^0\right). \tag{2}$$

In (2), $\psi_i^0 = \frac{V_i}{d_i^0}$ and $\psi_j^0 = \frac{V_j}{d_j^0}$, where d_i^0 is the real distance between the anchor node and the mobile node, and d_j^0 is the real distance between the ordinary node and the mobile node,which can be expressed as

$$\begin{aligned} d_i^0 &= \left\|\boldsymbol{u}^0 - \boldsymbol{s}_i\right\| \\ &= \sqrt{(x-x_i)^2 + (y-y_i)^2 + (z-z_i)^2}, \end{aligned} \tag{3}$$

$$\begin{aligned} d_j^0 &= \left\|\boldsymbol{u}^0 - \boldsymbol{n}_j\right\| \\ &= \sqrt{\left(x-x_j\right)^2 + \left(y-y_j\right)^2 + \left(z-z_j\right)^2}, \end{aligned} \tag{4}$$

$$\begin{aligned} V_i &= \left(\boldsymbol{u}^0 - \boldsymbol{s}_i\right)^T \boldsymbol{v}^0 \\ &= (x-x_i)\, v_x + (y-y_i)\, v_y + (z-z_i)\, v_z, \end{aligned} \tag{5}$$

and

$$\begin{aligned} V_j &= \left(\boldsymbol{u}^0 - \boldsymbol{s}_j\right)^T \boldsymbol{v}^0 \\ &= \left(x-x_j\right) v_x + \left(y-y_j\right) v_y + \left(z-z_j\right) v_z. \end{aligned} \tag{6}$$

Then, the ordinary node j obtains the Doppler shift between the monitoring signal transmitted by anchor node i and the reflected signal by the mobile node is

$$f_{ij}^0 = f_{ci} - f_{i,j}, \tag{7}$$

To be exact, the Doppler shift observation equation obtained by ordinary node j can be expressed as

$$f_{ij}^0 = \frac{f_{ci}}{c}\left(\psi_i^0 + \psi_j^0\right). \tag{8}$$

In view of the measurement error in the actual underwater environment, the Doppler shift measurement value has

$$f_{ij} = f_{ij}^0 + \Delta f_{ij}, \tag{9}$$

where f_{ij}, f_{ij}^0, Δf_{ij} are the measured value, true value, and measurement error of the Doppler shift, respectively. For Δf_{ij}, corresponding verification analysis has been given in [23], [24], which proves that when the Doppler shift is estimated in the presence of environmental noise and multi-path effect, the Doppler shift estimation error approximately obeys the zero-mean Gaussian distribution. The measurement of the Doppler shift can be modeled as

$$\boldsymbol{f} = \boldsymbol{f}^0 + \Delta \boldsymbol{f}. \tag{10}$$

In (10), $\boldsymbol{f}$ is the Doppler shift measurement vector, $\boldsymbol{f}^0$ and $\Delta \boldsymbol{f}$ are the Doppler shift reference (a vector composed of the true values of the Doppler shift) and the Doppler shift measurement error, respectively. The vector in the above formula can be expressed written as

$$\boldsymbol{f} = \left[\boldsymbol{f}_1^T, \boldsymbol{f}_2^T, \boldsymbol{f}_3^T, \cdots, \boldsymbol{f}_N^T\right]^T \tag{11a}$$

$$\boldsymbol{f}_j = \boldsymbol{f}_j^0 + \Delta \boldsymbol{f}_j \tag{11b}$$

$$\boldsymbol{f}_j = \left[f_{1j}, f_{2j}, f_{3j}, \cdots, f_{Mj}\right]^T \tag{11c}$$

$$\Delta \boldsymbol{f}_j = \left[\Delta f_{1j}, \Delta f_{2j}, \Delta f_{3j}, \cdots, \Delta f_{Mj}\right]^T. \tag{11d}$$

As shown in Fig. 2, the AOA observation equation of ordinary node j when the reflected signal reaches the ordinary node is expressed as

$$\alpha_j^0 = \arctan\frac{y - y_j}{x - x_j} \tag{12}$$

and

$$\beta_j^0 = \arcsin\frac{z - z_j}{d_j^0}. \tag{13}$$

In (12) and (13), α_j^0 and β_j^0 are the real azimuth and elevation of the mobile node relative to the j-th ordinary node, respectively, where $\alpha_j^0 \in (-\pi, \pi]$, $\beta_j^0 \in (0, \pi/2)$; considering the influence of measurement error, the measured values of azimuth and elevation are

$$\alpha_j = \alpha_j^0 + \Delta\alpha_j \tag{14}$$

and

$$\beta_j = \beta_j^0 + \Delta\beta_j. \tag{15}$$

In (14) and (15), $\Delta\alpha_j$ is the measurement error of the azimuth α_j and $\Delta\beta_j$ is the measurement error of the elevation β_j. The AOA obtained by the ordinary nodes can be expressed in vector form, where $\boldsymbol{\alpha} = [\alpha_1, \alpha_2, \alpha_3, \cdots, \alpha_N]^T$ and $\boldsymbol{\beta} = [\beta_1, \beta_2, \beta_3, \cdots, \beta_N]^T$ for $j = 1, 2, \cdots, N$, and (14) and (15) can be further expressed as

$$\boldsymbol{\alpha} = \boldsymbol{\alpha}^0 + \Delta\boldsymbol{\alpha} \tag{16}$$

and

$$\boldsymbol{\beta} = \boldsymbol{\beta}^0 + \Delta\boldsymbol{\beta}. \tag{17}$$

where $\boldsymbol{\alpha}$ is the azimuth measurement vector, $\boldsymbol{\alpha}^0$ and $\Delta\boldsymbol{\alpha}$ are the azimuth reference value (a vector composed of the true values of the azimuth) and the azimuth measurement error vector, respectively. $\boldsymbol{\beta}$ is the elevation measurement vector, $\boldsymbol{\beta}^0$ and $\Delta\boldsymbol{\beta}$ are the elevation reference value (the vector formed by the true value of elevation angle) and the elevation measurement error vector, respectively.

In summary, to simplify the algorithm derivation process, MN Doppler shift measurements and N pairs of AOA measurement information obtained by ordinary nodes are collected. The Doppler shift and AOA measurement information are recorded as $\boldsymbol{\varepsilon}$, and the observation vector $\boldsymbol{\varepsilon}$ can be recorded as follow:

$$\boldsymbol{\varepsilon} = \left[\boldsymbol{f}^T, \boldsymbol{\alpha}^T, \boldsymbol{\beta}^T\right]^T. \tag{18}$$

Combining (10), (16), and (17), the measurement equation of the method localization on the mobile node is

$$\boldsymbol{\varepsilon} = \boldsymbol{\varepsilon}^0 + \Delta\boldsymbol{\varepsilon}. \tag{19}$$

In (19), $\boldsymbol{\varepsilon}^0 = \left[\boldsymbol{f}^{0^T}, \boldsymbol{\alpha}^{0^T}, \boldsymbol{\beta}^{0^T}\right]^T$ is the observation vector without measurement error, and $\Delta\boldsymbol{\varepsilon} = \left(\Delta\boldsymbol{f}^T, \Delta\boldsymbol{\alpha}^T, \Delta\boldsymbol{\beta}^T\right)^T$ is the corresponding measurement error vector. It is assumed that $\Delta\boldsymbol{\varepsilon}$ obeys a Gaussian distribution with a mean value of zero. The covariance matrix of $\Delta\boldsymbol{\varepsilon}$ is $\boldsymbol{Q}_{\boldsymbol{\varepsilon}} = E\left[\Delta\boldsymbol{\varepsilon}\Delta\boldsymbol{\varepsilon}^T\right] = \mathrm{diag}\left(\boldsymbol{Q}_{\boldsymbol{f}}, \boldsymbol{Q}_{\boldsymbol{\alpha}}, \boldsymbol{Q}_{\boldsymbol{\beta}}\right)$, and $\boldsymbol{Q}_{\boldsymbol{f}}$, $\boldsymbol{Q}_{\boldsymbol{\alpha}}$, and $\boldsymbol{Q}_{\boldsymbol{\beta}}$ are the covariance matrices corresponding to the measurement error vectors $\Delta\boldsymbol{f}$, $\Delta\boldsymbol{\alpha}$, and $\Delta\boldsymbol{\beta}$, respectively.

For the mobile node, the unknown position and velocity information is expressed as $\boldsymbol{\Theta} = \left[\boldsymbol{u}^{0^T}, \boldsymbol{v}^{0^T}\right]^T$. The algorithm proposed in this article uses MN Doppler shift measurements, N azimuth measurements, and N elevation measurements with measurement errors, combined with the statistical characteristics of the error corresponding to each type of measurement parameter. Based on the measurement model, the algorithm estimates localization information of the mobile node as accurately as possible.

IV. DAHL ALGORITHM

The DAHL algorithm uses a two-stage estimation process. Since there is a nonlinear relationship between observation vector $\boldsymbol{\varepsilon}$ and the unknown parameter $\boldsymbol{\Theta}$ of the mobile node, in the first stage, using the obtained Doppler shift and AOA measurement data, construct a pseudolinear equation about $\boldsymbol{u}^0$ and $\boldsymbol{v}^0$ of the mobile node and observation vector $\boldsymbol{\varepsilon}$ to solve the existing nonlinear problem and preliminarily estimate the position and velocity of the mobile node. In the second stage, the relationship between the auxiliary parameters and the parameters of the mobile node is used to optimize the estimation error in the first stage.

A. FIRST STAGE

In DAHL, regardless of the position error of the anchor node and the ordinary node, each ordinary node can accurately measure the arrival time of the monitoring signal and the mobile node reflecting signal. The distance difference between the two types of signal propagation can be expressed as

$$r_{ij} = d_i^0 + d_j^0 - d_{ij}. \tag{20}$$

In (20), r_{ij} can be obtained by the product of the time difference between the arrival time of the signal and the speed of underwater acoustics, i.e., $r_{ij} = c\tau_{ij}$. d_{ij} is the distance between the anchor node and the ordinary node, and d_{ij} is obtained by

$$\begin{aligned} d_{ij} &= \left\|\boldsymbol{s}_i - \boldsymbol{n}_j\right\| \\ &= \sqrt{\left(x_i - x_j\right)^2 + \left(y_i - y_j\right)^2 + \left(z_i - z_j\right)^2}. \end{aligned} \tag{21}$$

Substituting (8) into (9) and shifting the terms; then, substituting (20) to obtain

$$\begin{aligned} cd_i^0\Delta f_{ij} = {} & cr_{ij}f_{ij} + cd_{ij}f_{ij} - f_{ci}\left(\boldsymbol{n}_j - \boldsymbol{s}_i\right)^T\boldsymbol{v}^0 \\ & - f_{ci}\psi_j^0\left(r_{ij} + d_{ij}\right) - cd_j^0 f_{ij}. \end{aligned} \tag{22}$$

For the azimuth and elevation measurements, this article assumes that the measurement error of the two parameters is small, which can be written as

$$\Delta\alpha_j = \alpha_j - \alpha_j^0 \approx 0 \tag{23}$$

and

$$\Delta\beta_j = \beta_j - \beta_j^0 \approx 0. \tag{24}$$

According to (23) and (24), $\cos\Delta\alpha_j \approx 1$, $\sin\Delta\alpha_j \approx \Delta\alpha_j$, $\cos\Delta\beta_j \approx 1$, and $\sin\Delta\beta_j \approx \Delta\beta_j$ can be clearly obtained.

Similar to [25], substituting (14) and (15) into (12) and (13), respectively, to obtain

$$\mathbf{g}_j^T\left(\boldsymbol{n}_j - \boldsymbol{u}^0\right)\Delta\alpha_j = \boldsymbol{q}_j^T\boldsymbol{u}^0 - \boldsymbol{q}_j^T\boldsymbol{n}_j \tag{25}$$

and

$$\boldsymbol{d}_j^0\cos\beta_j\Delta\beta_j = \boldsymbol{m}^T\boldsymbol{n}_j - \boldsymbol{m}^T\boldsymbol{u}^0 + \boldsymbol{d}_j^0\sin\beta_j. \tag{26}$$

In (25), $\mathbf{g}_j$ and $\boldsymbol{q}_j$ are expressed as $\left[\cos\alpha_j, \sin\alpha_j, 0\right]^T$ and $\left[\sin\alpha_j, -\cos\alpha_j, 0\right]^T$, and in (26), $\boldsymbol{m} = [0, 0, 1]^T$.

In this stage, with the help of auxiliary parameters $\boldsymbol{\psi}^0$ and $\boldsymbol{\mu}^0$, an approximately linear relationship can be established between the position parameters $\boldsymbol{u}^0$ and $\boldsymbol{v}^0$ of the mobile node and the observation vector $\boldsymbol{\varepsilon}$ of the ordinary node. Therefore, the estimated parameter vector is recorded as $\boldsymbol{\gamma}_0 = \left[\boldsymbol{u}^{0^T}, \boldsymbol{v}^{0^T}, \boldsymbol{\psi}^{0^T}, \boldsymbol{\mu}^{0^T}\right]^T$, where $\boldsymbol{\gamma}_0$ includes $2N+6$ parameters; where $\boldsymbol{\psi}^0 = \left[\frac{V_1}{d_1^0}, \frac{V_2}{d_2^0}, \cdots, \frac{V_N}{d_N^0}\right]^T$ and $\boldsymbol{\mu}^0 = \left[d_1^0, d_2^0, \cdots, d_N^0\right]^T$, and each unknown parameter is independent of each other.

Combining (22), (25), and (26), the relationship between the observation vector obtained by different ordinary nodes and the estimated parameter vector can be written as the following linear equation:

$$\boldsymbol{B}_1\Delta\boldsymbol{\varepsilon} = \boldsymbol{h}_1 - \boldsymbol{G}_1\boldsymbol{\gamma}_0, \tag{27}$$

where

$$\boldsymbol{B}_1 = \left[\ \text{blkdiag}\ \left(\boldsymbol{B}_{1f}, \boldsymbol{B}_{1\alpha}, \boldsymbol{B}_{1\beta}\right)\right] \tag{28a}$$

$$\boldsymbol{B}_{1f} = c\boldsymbol{I}_N \otimes \text{diag}\left(d_1^0, d_2^0, \cdots, d_M^0\right) \tag{28b}$$

$$\boldsymbol{B}_{1\alpha} = \text{diag}\left(\mathbf{g}_1^T\left(\boldsymbol{n}_1 - \boldsymbol{u}^0\right), \cdots, \mathbf{g}_N^T\left(\boldsymbol{n}_N - \boldsymbol{u}^0\right)\right) \tag{28c}$$

$$\boldsymbol{B}_{1\beta} = \text{diag}\left(d_1^0 \cos\beta_1, \cdots, d_N^0 \cos\beta_N\right), \tag{28d}$$

$$\boldsymbol{h}_1 = \left[\boldsymbol{h}_{1f}^T, \boldsymbol{h}_{1\alpha}^T, \boldsymbol{h}_{1\beta}^T\right]^T \tag{29a}$$

$$\boldsymbol{h}_{1f} = \left[\boldsymbol{h}_{1f,1}^T, \boldsymbol{h}_{1f,2}^T, \cdots, \boldsymbol{h}_{1f,M}^T\right]^T \tag{29b}$$

$$\boldsymbol{h}_{1f,i} = \left[cf_{i1}\left(d_{i1} + r_{i1}\right), \cdots, cf_{iN}\left(d_{iN} + r_{iN}\right)\right]^T \tag{29c}$$

$$\boldsymbol{h}_{1\alpha} = \left[-\boldsymbol{q}_1^T\boldsymbol{n}_1, -\boldsymbol{q}_2^T\boldsymbol{n}_2, \cdots, -\boldsymbol{q}_N^T\boldsymbol{n}_N\right]^T \tag{29d}$$

$$\boldsymbol{h}_{1\beta} = \left[\boldsymbol{m}^T\boldsymbol{n}_1, \boldsymbol{m}^T\boldsymbol{n}_2, \cdots, \boldsymbol{m}^T\boldsymbol{n}_N\right]^T, \tag{29e}$$

and

$$\boldsymbol{G}_1 = \left[\boldsymbol{G}_{1f}^T, \boldsymbol{G}_{1\alpha}^T, \boldsymbol{G}_{1\beta}^T\right]^T \tag{30a}$$

$$\boldsymbol{G}_{1f} = \left[\boldsymbol{G}_{1f_1}, \boldsymbol{G}_{1f_j}\right] \tag{30b}$$

$$\boldsymbol{G}_{1f_1} = \left[\mathbf{0}_3^T, f_{ci}\left(\boldsymbol{n}_j - \boldsymbol{s}_i\right)^T, \mathbf{0}_{j-1}^T, f_{ci}\left(d_{ij} + r_{ij}\right)\right] \tag{30c}$$

$$\boldsymbol{G}_{1f_2} = \left[\mathbf{0}_{j-1}^T, cf_{ij}, \mathbf{0}_{N-1}^T\right] \tag{30d}$$

$$\boldsymbol{G}_{1\alpha} = \left[-\boldsymbol{q}_j^T, \mathbf{0}_{2N+3}^T\right] \tag{30e}$$

$$\boldsymbol{G}_{1\beta} = \left[\boldsymbol{m}^T, \mathbf{0}_{N+j+2}^T - \sin\beta_j, \mathbf{0}_{N-j}^T\right]. \tag{30f}$$

Based on (27), unknown parameter $\boldsymbol{\gamma}_0$ in the first stage can be estimated using weighted least squares. In the actual calculation process, the initial value of weighting matrix $\boldsymbol{W}$ needs to be set to obtain the estimated values of $\boldsymbol{u}_0$ and $\boldsymbol{v}_0$. Therefore, $\boldsymbol{Q}_{\boldsymbol{\varepsilon}}^{-1}$ is first set to $\boldsymbol{W}$ to generate the initial estimate of the mobile node state $\widehat{\boldsymbol{\gamma}}_0$, which can be expressed as

$$\widehat{\boldsymbol{\gamma}}_0 = \left(\boldsymbol{G}_1^T\boldsymbol{W}\boldsymbol{G}_1\right)^{-1}\boldsymbol{G}_1^T\boldsymbol{W}\boldsymbol{h}_1. \tag{31}$$

By substituting the estimated values of each parameter in $\boldsymbol{\gamma}_0$ into (28), (29), and (30), the matrix $\widehat{\boldsymbol{B}}_1$ is constructed to obtain a more accurate weighting matrix

$$\boldsymbol{W}_1 = \widehat{\boldsymbol{B}}_1^{-T}\boldsymbol{E}\left(\Delta\boldsymbol{\varepsilon}\Delta\boldsymbol{\varepsilon}^T\right)^{-1}\widehat{\boldsymbol{B}}_1^{-1} = \widehat{\boldsymbol{B}}_1^{-T}\boldsymbol{Q}_{\boldsymbol{\varepsilon}}^{-1}\widehat{\boldsymbol{B}}_1^{-1}. \tag{32}$$

Then, the weighted least squares estimated value $\boldsymbol{\gamma}_1$ of the unknown parameter $\boldsymbol{\gamma}_0$ in the first stage can be obtained as

$$\boldsymbol{\gamma}_1 = \left(\boldsymbol{G}_1^T\boldsymbol{W}_1\boldsymbol{G}_1\right)^{-1}\boldsymbol{G}_1^T\boldsymbol{W}_1\boldsymbol{h}_1. \tag{33}$$

The error covariance matrix of estimated parameter $\boldsymbol{\gamma}_1$ obtained in the first stage is $\text{cov}\left(\boldsymbol{\gamma}_1\right) \approx \left(\boldsymbol{G}_1^T\boldsymbol{W}_1\boldsymbol{G}_1\right)^{-1}$.

According to the above calculation, the estimated value of position vector $\boldsymbol{u}^0$ of the mobile node is $\widehat{\boldsymbol{u}} = \boldsymbol{\gamma}_1(1:3)$, and the estimated value of velocity vector $\boldsymbol{v}^0$ is $\widehat{\boldsymbol{v}} = \boldsymbol{\gamma}_1(4:6)$. In the practical application of underwater localization, the requirements for node localization accuracy are relatively high. Therefore, the estimated value of the first stage needs to be corrected to obtain an accurate estimation of the node position and velocity information.

B. SECOND STAGE

Record the estimated value obtained in the first stage as $\boldsymbol{\gamma}_1 = \left[\widehat{\boldsymbol{u}}^T, \widehat{\boldsymbol{v}}^T, \widehat{\boldsymbol{\psi}}^T, \widehat{\boldsymbol{\mu}}^T\right]^T$. The relationship between estimated value $\boldsymbol{\gamma}_1$ and true value $\boldsymbol{\gamma}_0$ can be written as

$$\boldsymbol{\gamma}_1 = \boldsymbol{\gamma}_0 + \Delta\boldsymbol{\gamma}_1. \tag{34}$$

In (34), $\Delta\boldsymbol{\gamma}_1 = \left(\Delta\boldsymbol{u}^T, \Delta\boldsymbol{v}^T, \Delta\boldsymbol{\psi}^T, \Delta\boldsymbol{\mu}^T\right)^T$ is the error vector corresponding to $\boldsymbol{\gamma}_1$, where $\Delta\boldsymbol{\psi} = \left[\Delta\psi_1, \Delta\psi_2 \cdots, \Delta\psi_N\right]^T$ and $\Delta\boldsymbol{\mu} = \left[\Delta d_1, \Delta d_2 \cdots, \Delta d_N\right]^T$. The vector contained in $\Delta\boldsymbol{\gamma}_1$ can be written as

$$\Delta\boldsymbol{u} = \widehat{\boldsymbol{u}} - \boldsymbol{u}^0 \tag{35a}$$

$$\Delta\boldsymbol{v} = \widehat{\boldsymbol{v}} - \boldsymbol{v}^0 \tag{35b}$$

$$\Delta\psi_j = \widehat{\psi}_j - \psi_j^0 \tag{35c}$$

$$\Delta d_j = \widehat{d}_j - d_j^0. \tag{35d}$$

In (35a) and (35b), $\Delta\boldsymbol{u}$ and $\Delta\boldsymbol{v}$ are the corrections of the position and velocity estimation, respectively. According to the error correction method proposed in [26], the two equations can be expressed as

$$\Delta\boldsymbol{u} = \mathbf{0}_3 + \Delta\boldsymbol{u} \tag{36}$$

and

$$\Delta\boldsymbol{v} = \mathbf{0}_3 + \Delta\boldsymbol{v}. \tag{37}$$

Equation (35d) is shifted, and both sides of the equation are squared at the same time. After ignoring the second-order estimation error, the following can be obtained that

$$2\widehat{d}_j\Delta d_j = \widehat{d}_j^2 - \widehat{\boldsymbol{u}}^T\widehat{\boldsymbol{u}} - \boldsymbol{n}_j^T\boldsymbol{n}_j + 2\widehat{\boldsymbol{u}}^T\boldsymbol{n}_j + 2\left(\widehat{\boldsymbol{u}} - \boldsymbol{n}_j\right)^T\Delta\boldsymbol{u}. \tag{38}$$

Similarly, after shifting (35c), it can be multiplied by the transformed (35d) to obtain

$$\widehat{d}_j\Delta\psi_j + \widehat{\psi}_j\Delta d_j = \widehat{d}_j\widehat{\psi}_j - \widehat{\boldsymbol{u}}^T\widehat{\boldsymbol{v}} + \boldsymbol{n}_j^T\widehat{\boldsymbol{v}} + \widehat{\boldsymbol{v}}^T\Delta\boldsymbol{u} + \left(\widehat{\boldsymbol{u}}^T - \boldsymbol{n}_j^T\right)\Delta\boldsymbol{v}. \tag{39}$$

Define the parameter to be estimated at this stage as $\Delta\boldsymbol{\delta} = \left[\Delta\boldsymbol{u}^T, \Delta\boldsymbol{v}^T\right]^T$, based on the above discussion, combine (38) and (39) into

$$\boldsymbol{B}_2\Delta\boldsymbol{\gamma}_1 = \boldsymbol{h}_2 - \boldsymbol{G}_2\Delta\boldsymbol{\delta}. \tag{40}$$

In (40), the matrices $\boldsymbol{B}_2$, $\boldsymbol{h}_2$, and $\boldsymbol{G}_2$ are written as

$$\boldsymbol{B}_2 = \left[\boldsymbol{B}_{21}^T, \boldsymbol{B}_{22}^T, \boldsymbol{B}_{23}^T, \boldsymbol{B}_{24}^T\right]^T \tag{41a}$$

$$\boldsymbol{B}_{21} = \left[\boldsymbol{I}_{3\times3}, \mathbf{0}_{(2N+3)\times3}^T\right] \tag{41b}$$

$$\boldsymbol{B}_{22} = \left[\mathbf{0}_{3\times3}^T, \boldsymbol{I}_{3\times3}, \mathbf{0}_{(2N)\times3}^T\right] \tag{41c}$$

$$\boldsymbol{B}_{23} = \left[\mathbf{0}_{N\times6}, \text{diag}\left(\widehat{d}_j\right), \text{diag}\left(\widehat{\psi}_j\right)\right] \tag{41d}$$

$$\boldsymbol{B}_{24} = \left[\mathbf{0}_{N\times(N+6)}, 2\,\text{diag}\left(\widehat{d}_j\right)\right], \tag{41e}$$

$$\boldsymbol{h}_2 = \left[\boldsymbol{0}_{1\times3}^T, \boldsymbol{0}_{1\times3}^T, \boldsymbol{h}_{2f}^T, \boldsymbol{h}_{2d}^T\right]^T \tag{42a}$$
$$\boldsymbol{h}_{2f} = \widehat{d}_j\widehat{\psi}_j - \widehat{\boldsymbol{u}}^T\widehat{\boldsymbol{v}} + \boldsymbol{n}_j^T\widehat{\boldsymbol{v}} \tag{42b}$$
$$\boldsymbol{h}_{2d} = \widehat{d}_j^2 - \widehat{\boldsymbol{u}}^T\widehat{\boldsymbol{u}} - \boldsymbol{n}_j^T\boldsymbol{n}_j + 2\widehat{\boldsymbol{u}}^T\boldsymbol{n}_j, \tag{42c}$$

and

$$\boldsymbol{G}_2 = \left[\boldsymbol{G}_{21}^T, \boldsymbol{G}_{22}^T, \boldsymbol{G}_{23}^T, \boldsymbol{G}_{24}^T\right]^T \tag{43a}$$
$$\boldsymbol{G}_{21} = [-\boldsymbol{I}_{3\times3}, \boldsymbol{0}_{3\times3}] \tag{43b}$$
$$\boldsymbol{G}_{22} = [\boldsymbol{0}_{3\times3} - \boldsymbol{I}_{3\times3}] \tag{43c}$$
$$\boldsymbol{G}_{23} = \left[-\widehat{\boldsymbol{v}}^T, -\left(\widehat{\boldsymbol{u}} - \boldsymbol{n}_j\right)^T\right] \tag{43d}$$
$$\boldsymbol{G}_{24} = \left[-2\left(\widehat{\boldsymbol{u}} - \boldsymbol{n}_j\right)^T, \boldsymbol{0}_{N\times3}\right]. \tag{43e}$$

Let the estimated value of $\Delta\boldsymbol{\delta}$ be $\boldsymbol{\gamma}_2$; through (40), the weighted least squares estimate of the parameter to be estimated in the second stage of $\Delta\boldsymbol{\delta}$ can be obtained by

$$\boldsymbol{\gamma}_2 = \Delta\widehat{\boldsymbol{\delta}} = \left(\boldsymbol{G}_2^T\boldsymbol{W}_2\boldsymbol{G}_2\right)^{-1}\boldsymbol{G}_2^T\boldsymbol{W}_2\boldsymbol{h}_2, \tag{44}$$

where $\boldsymbol{W}_2$ is a weighted matrix, which is

$$\begin{aligned}\boldsymbol{W}_2 &= \boldsymbol{B}_2^{-T}\boldsymbol{E}\left(\Delta\boldsymbol{\gamma}_1\Delta\boldsymbol{\gamma}_1^T\right)^{-1}\boldsymbol{B}_2^{-1} \\ &= \boldsymbol{B}_2^{-T}\,\mathrm{cov}\left(\boldsymbol{\gamma}_1\right)^{-1}\boldsymbol{B}_2^{-1}.\end{aligned} \tag{45}$$

The covariance matrix of $\boldsymbol{\gamma}_2$ is

$$\mathrm{cov}\left(\boldsymbol{\gamma}_2\right) = \left(\boldsymbol{G}_2^T\boldsymbol{W}_2\boldsymbol{G}_2\right)^{-1}. \tag{46}$$

After the correction by (44), $\Delta\widehat{\boldsymbol{u}} = \boldsymbol{\gamma}_2(1:3)$ and $\Delta\widehat{\boldsymbol{v}} = \boldsymbol{\gamma}_2(4:6)$ can be obtained. According to the established relationships in (35a) and (35b), the position and velocity can be estimated as

$$\tilde{\boldsymbol{u}} = \widehat{\boldsymbol{u}} - \Delta\widehat{\boldsymbol{u}} \tag{47}$$

and

$$\tilde{\boldsymbol{v}} = \widehat{\boldsymbol{v}} - \Delta\widehat{\boldsymbol{v}}. \tag{48}$$

The obtained position and velocity estimates of the mobile node are written as $\widetilde{\boldsymbol{\delta}} = \left[\widetilde{\boldsymbol{u}}^T, \widetilde{\boldsymbol{\gamma}}^T\right]^T$, and the covariance matrix of $\widetilde{\boldsymbol{\delta}}$ is

$$\begin{aligned}\mathrm{cov}(\widetilde{\boldsymbol{\delta}}) &= \mathrm{cov}\left(\boldsymbol{\gamma}_2\right) \\ &= \left(\boldsymbol{G}_2^T\boldsymbol{B}_2^{-T}\boldsymbol{G}_1^T\boldsymbol{B}_1^{-T}\boldsymbol{Q}_\varepsilon^{-1}\boldsymbol{B}_1^{-1}\boldsymbol{G}_1\boldsymbol{B}_2^{-1}\boldsymbol{G}_2\right)^{-1}.\end{aligned} \tag{49}$$

V. CRLB ANALYSIS

The previous section discussed the DAHL algorithm for the estimation process of the localization information of the mobile node in detail. This section will conduct a theoretical analysis of the DAHL algorithm, verify the effectiveness of the proposed algorithm, and give the CRLB of the estimation error to establish the performance limit of the mobile node location problem.

The CRLB of the position and velocity estimation in this article can be obtained by calculating the inverse of the Fisher information matrix (FIM) [27]. Since the measured values of the Doppler shift and AOA satisfy the measurement model in (19), and the Doppler shift and AOA measurement error $\Delta\boldsymbol{\varepsilon}$ obey the Gaussian distribution with zero mean, the mixed Gaussian probability density function based on the Doppler shift and AOA measurement is

$$\mathbf{P}(\boldsymbol{\varepsilon} \mid \boldsymbol{\Theta}) = \boldsymbol{K}e^{-\frac{1}{2}\left(\boldsymbol{\varepsilon}-\boldsymbol{\varepsilon}^0\right)^T\boldsymbol{Q}_\varepsilon^{-1}\left(\boldsymbol{\varepsilon}-\boldsymbol{\varepsilon}^0\right)}, \tag{50}$$

where $\boldsymbol{K}$ is the normalization constant. FIM of $\boldsymbol{\Theta}$ can be expressed as

$$\boldsymbol{F} = \boldsymbol{J}(\boldsymbol{\Theta})^T\boldsymbol{Q}_{\boldsymbol{\varepsilon}}^{-1}\boldsymbol{J}(\boldsymbol{\Theta}). \tag{51}$$

In (51), $\boldsymbol{J}(\boldsymbol{\Theta})$ is the Jacobian matrix, which can be expressed as

$$\boldsymbol{J}(\boldsymbol{\Theta}) = \nabla_{\boldsymbol{\theta}}^{\varepsilon^0} = \begin{bmatrix} \frac{\partial \boldsymbol{f}^0}{\partial \boldsymbol{u}^{0T}} & \frac{\partial \boldsymbol{f}^0}{\partial \boldsymbol{v}^{0T}} \\ \frac{\partial \boldsymbol{\alpha}^0}{\partial \boldsymbol{u}^{0T}} & \boldsymbol{0} \\ \frac{\partial \boldsymbol{\beta}^0}{\partial \boldsymbol{u}^{0T}} & \boldsymbol{0} \end{bmatrix}, \tag{52}$$

where

$$\frac{\partial \boldsymbol{f}^0}{\partial \boldsymbol{u}^{0T}} = \frac{f_{ci}}{c}\left(\frac{\partial \psi_i^0}{\partial \boldsymbol{u}^{0T}} + \frac{\partial \psi_j^0}{\partial \boldsymbol{u}^{0T}}\right) \tag{53a}$$
$$\frac{\partial \psi_i^0}{\partial \boldsymbol{u}^{0T}} = \frac{\boldsymbol{v}^0}{\left\|\boldsymbol{u}^0 - \boldsymbol{s}_i\right\|} - \frac{\left(\boldsymbol{u}^0 - \boldsymbol{s}_i\right)^T\boldsymbol{v}^0}{\left\|\boldsymbol{u}^0 - \boldsymbol{s}_i\right\|^2}\frac{\left(\boldsymbol{u}^0 - \boldsymbol{s}_i\right)^T}{\left\|\boldsymbol{u}^0 - \boldsymbol{s}_i\right\|} \tag{53b}$$
$$\frac{\partial \psi_j^0}{\partial \boldsymbol{u}^{0T}} = \frac{\boldsymbol{v}^0}{\left\|\boldsymbol{u}^0 - \boldsymbol{n}_j\right\|} - \frac{\left(\boldsymbol{u}^0 - \boldsymbol{n}_j\right)^T\boldsymbol{v}^0}{\left\|\boldsymbol{u}^0 - \boldsymbol{n}_j\right\|^2}\frac{\left(\boldsymbol{u}^0 - \boldsymbol{n}_j\right)^T}{\left\|\boldsymbol{u}^0 - \boldsymbol{n}_j\right\|} \tag{53c}$$
$$\frac{\partial \boldsymbol{f}^0}{\partial \boldsymbol{v}^{0T}} = \frac{f_{ci}}{c}\left(\frac{\left(\boldsymbol{u}^0 - \boldsymbol{s}_i\right)^T}{\left\|\boldsymbol{u}^0 - \boldsymbol{s}_i\right\|} + \frac{\left(\boldsymbol{u}^0 - \boldsymbol{n}_j\right)^T}{\left\|\boldsymbol{u}^0 - \boldsymbol{n}_j\right\|}\right) \tag{53d}$$
$$\frac{\partial \boldsymbol{\alpha}^0}{\partial \boldsymbol{u}^{0T}} = \frac{\left[-\sin\alpha_j^0, \cos\alpha_j^0, 0\right]}{\left\|\boldsymbol{u}^0 - \boldsymbol{s}_i\right\|^2} \tag{53e}$$
$$\frac{\partial \boldsymbol{\beta}^0}{\partial \boldsymbol{u}^{0T}} = \left[0, 0, \frac{1}{\left\|\boldsymbol{u}^0 - \boldsymbol{n}_j\right\|\cos\beta_j^0}\right]. \tag{53f}$$

Then, the CRLB of $\boldsymbol{\Theta}$ can be obtained as

$$CRLB(\boldsymbol{\Theta}) = \left(\boldsymbol{J}(\boldsymbol{\Theta})^T\boldsymbol{Q}_\varepsilon^{-1}\boldsymbol{J}(\boldsymbol{\Theta})\right)^{-1}. \tag{54}$$

Equation (54) includes the CRLB for the position and velocity estimation. It should be noted that the small errors mentioned in this article are $\Delta f_{ij} \ll f_{ij}$, $c\Delta f_{ij} \ll d_i^0$, $\Delta\alpha_j \approx 0$, and $\Delta\beta_i \approx 0$. When the above conditions are met, the proposed method can theoretically achieve the CRLB.

VI. SIMULATION RESULTS

The localization performance of the DAHL algorithm will be verified through simulation experiments in this section.

A. PERFORMANCE METRICS

In this article, the CRLB is used as the evaluation standard for evaluating localization performance, and the root mean square error (RMSE) is used as the evaluation

index to measure the accuracy of the position and velocity estimation. The RMSE is defined as

$$\mathrm{RMSE}_{\boldsymbol{u}} = \sqrt{\frac{1}{L}\sum_{l=1}^{L}\left\|\boldsymbol{u}^0 - \tilde{\boldsymbol{u}}_l\right\|^2} \tag{55a}$$

$$\mathrm{RMSE}_{\boldsymbol{v}} = \sqrt{\frac{1}{L}\sum_{l=1}^{L}\left\|\boldsymbol{v}^0 - \tilde{\boldsymbol{v}}_l\right\|^2}, \tag{55b}$$

where L is the number of Monte Carlo simulations, and 1000 independent Monte Carlo simulations are performed for each experiment in the simulation. $\mathrm{RMSE}_{\boldsymbol{u}}$ represents the RMSE of the position, and $\mathrm{RMSE}_{\boldsymbol{v}}$ represents the RMSE of the velocity. $\tilde{\boldsymbol{u}}_l$ and $\tilde{\boldsymbol{v}}_l$ are the estimated values of the $\boldsymbol{u}_0$ and $\boldsymbol{v}_0$ obtained by the l-th Monte Carlo simulation experiment. It should be pointed out that in each simulation experiment, the trajectory of the mobile node is consistent.

B. SIMULATION SCENARIO

To achieve better performance of DAHL, this article makes a trade-off between the energy consumption of the anchor nodes vs. ordinary nodes and (in the experimental situation) the number of nodes vs. the localization accuracy. The localization ability of DAHL is tested by simulating a deployed localization network consisting of 3 anchor nodes and 5 ordinary nodes. These nodes in the network are accurately deployed in an area of 1000 m × 1000 m × 400 m, the maximum transmission range of anchors node is 1000 m, and the average speed of sound in water is 1500 m/s. The position of the mobile node to be located is $\boldsymbol{u}^0 = [600, 800, 300]^T$ m, and the velocity is $\boldsymbol{v}^0 = [2.4, 1.6, 1.2]^T$ m/s. The deployment positions of nodes used for localization in the network as shown in Table 1.

TABLE 1. Anchor node and ordinary node positions (in meters).

$\mathbf{s}_i$	f_{ci}	x_i	y_i	z_i	$\mathbf{n}_j$	x_j	y_j	z_j
1	10kHz	800	400	50	1	550	400	250
2	12kHz	500	700	100	2	500	300	200
3	14kHz	700	200	150	3	400	300	50
–	–	–	–	–	4	100	100	150
–	–	–	–	–	5	600	700	100

Since the propagation speed of underwater sound is much greater than the velocity of the mobile node, assuming that the mobile node reflects the monitoring signals emitted by each anchor node at the same location. The covariance matrix of measurement error $\Delta\boldsymbol{\varepsilon}$ is $\boldsymbol{Q}_{\boldsymbol{\varepsilon}} = \mathrm{diag}\left(\boldsymbol{Q}_{\boldsymbol{f}}, \boldsymbol{Q}_{\boldsymbol{\alpha}}, \boldsymbol{Q}_{\boldsymbol{\beta}}\right)$. The following assumptions are made about the measurement error contained in $\Delta\boldsymbol{\varepsilon}$: (1) Doppler shift measurement error $\Delta f_{ij} \sim N\left(0, \sigma_f^2\right)$, and the covariance matrix of $\Delta\boldsymbol{f}$ is $\boldsymbol{Q}_{\boldsymbol{f}} = \sigma_f^2\boldsymbol{I}_{MN\times MN}$; (2) azimuth measurement error $\Delta\alpha_j \sim N\left(0, \sigma_\alpha^2\right)$, and the covariance matrix of $\Delta\boldsymbol{\alpha}$ is $\boldsymbol{Q}_{\boldsymbol{\alpha}} = \sigma_\alpha^2\boldsymbol{I}_{N\times N}$; (3) elevation measurement error $\Delta\beta_j \sim N\left(0, \sigma_\beta^2\right)$, and the covariance matrix of $\Delta\boldsymbol{\beta}$ is $\boldsymbol{Q}_{\boldsymbol{\beta}} = \sigma_\beta^2\boldsymbol{I}_{N\times N}$; and (4) σ_f represents the standard deviation of the Doppler shift measurement error (i.e., the measurement error level of the Doppler shift), σ_α and σ_β represent the standard deviation of the azimuth and elevation measurement errors, respectively (in this article, $\sigma_\alpha = \sigma_\beta$ is assumed, σ_α and σ_β are uniformly expressed as σ_{AOA}, i.e., the AOA measurement error level), and the measurement error vectors $\Delta\boldsymbol{f}$, $\Delta\boldsymbol{\alpha}$, and $\Delta\boldsymbol{\beta}$ are not correlated with each other.

C. MOBILE NODE POSITION AND VELOCITY ESTIMATION

1) The LOCALIZATION ACCURACY OF THE ALGORITHM UNDER DIFFERENT MEASUREMENT ERROR CONDITIONS

In the simulation, the position and velocity estimation accuracy under different measurement error levels is evaluated to verify the localization performance of the DAHL algorithm for the mobile node. Set the variation range of σ_f and σ_{AOA} are 0.1 Hz to 10 Hz and 0.02 deg to 2 deg, respectively. To further verify the effectiveness of DAHL for mobile node localization, the following two localization algorithms are used as comparison algorithms: (1) the localization method based on BR and AOA proposed in [15] and (2) the DAHL algorithm without AOA measurement.

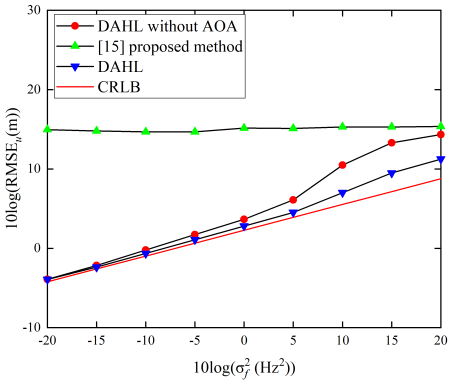

FIGURE 3. When the deviation of the AOA measurement error is 1 deg, the RMSE of the mobile node position estimate varies with σ_f.

Fig. 3 shows that when the AOA measurement error deviation is constant at 1 deg, the localization accuracy of the mobile node changes with the increase in the Doppler shift measurement error level. As shown in Fig. 3, the method proposed in [15] has poor localization accuracy for the mobile node. This is because when processing the localization of the mobile node, the method does not use the Doppler shift containing the position and velocity information of the mobile node. Although the localization accuracy of the parameter measurement is not affected by the change in Doppler shift measurement error, it ignores the interference caused by the velocity of the node to the localization, resulting in poor localization accuracy. The DAHL without the AOA localization method that uses the Doppler shift measurement to locate the mobile node is better than the method proposed in [15]. It can be seen from Fig. 3 that after introducing

the AOA measurement parameters into the solution that only uses Doppler shift localization, the DAHL method improves the localization accuracy of the mobile node accordingly. When $\sigma_f^2 = 0.1\text{Hz}^2$, the localization accuracy of the DAHL method gradually deviates from the CRLB, but with the increase in σ_f, the DAHL method shows better localization performance.

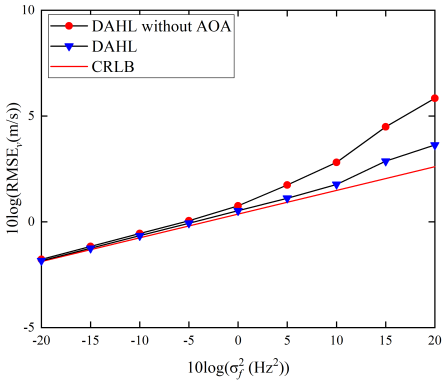

FIGURE 4. When the deviation of the AOA measurement error is 1 deg, the RMSE of the mobile node velocity estimate varies with σ_f.

Since the localization method in [15] cannot use measurement data to attain the velocity of the mobile node, when evaluating the performance of DAHL for mobile node velocity estimation, it is only compared with the DAHL without AOA method. Fig. 4 shows the comparison of the estimation accuracy of the mobile node velocity with the two localization methods as the Doppler shift measurement error level changes and the AOA measurement error deviation remains constant at 1 deg. And Fig. 4 shows that when the Doppler shift measurement error variance $\sigma_f^2 < 0.1\text{Hz}^2$, i.e., when the Doppler shift measurement error is small, the RMSE$_v$ of the DAHL method and the DAHL without AOA method is close to the CRLB. When $\sigma_f^2 > 0.1\text{Hz}^2$, the velocity estimation accuracy of the two algorithms for the mobile node starts to deviate from the CRLB. Compared with the DAHL without the AOA localization method, the RMSE$_v$ curve of the DAHL method for the mobile node velocity estimation deviates to a smaller degree from the CRLB, which shows that it has high velocity estimation accuracy.

It can be seen from Fig. 5 that when the Doppler shift measurement error deviation is constant at 2 Hz, the localization accuracy of the mobile node is the result of different AOA measurement error levels. The DAHL without the AOA method does not include AOA measurement parameters, so the change in AOA measurement error does not affect its localization accuracy. However, the method proposed in [15] is more seriously affected by AOA measurement error changes. The increasing AOA measurement error dominates the localization performance of this method, making its localization accuracy significantly lower than that of the DAHL without AOA method and DAHL method. In addition, it ignores the influence of the velocity of the mobile node

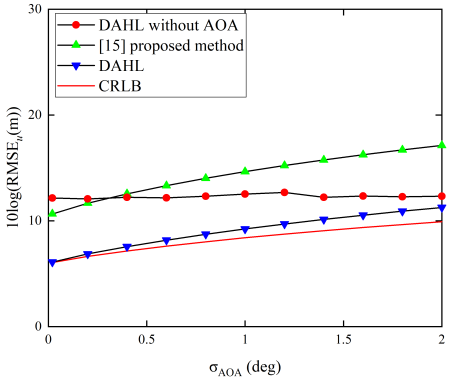

FIGURE 5. When the Doppler shift measurement error deviation is 2 Hz, the RMSE of the mobile node position estimate varies with σ_{AOA}.

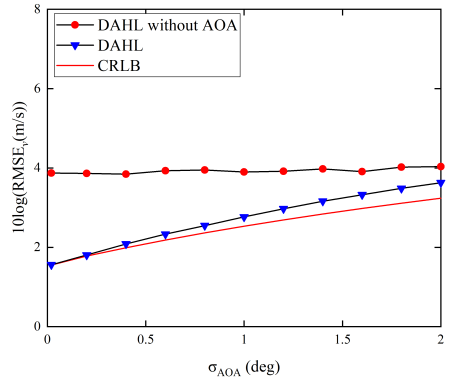

FIGURE 6. When the Doppler shift measurement error deviation is 2 Hz, the RMSE of the mobile node velocity estimate varies with σ_{AOA}.

on the localization, resulting in a large error in the localization accuracy. Compared with the other two algorithms, the DAHL method exhibits a higher localization accuracy in the process of increasing σ_{AOA}.

As shown in Fig. 6, when $\sigma_f = 2$ Hz, the RMSE$_v$ of the DAHL without AOA method for the mobile node is stable at approximately 4.6 m/s. This is because DAHL without the AOA localization method does not include AOA measurement parameters. In the process of estimating the velocity of the mobile node, the change in the AOA measurement error has no effect on the velocity estimation accuracy. Since σ_{AOA} has a small impact on the velocity estimation performance, when σ_f is constant at 2 Hz and the AOA measurement error is small, the RMSE$_v$ of DAHL for the mobile node is close to the CRLB. When $\sigma_{\text{AOA}} > 0.2$ deg, the RMSE$_v$ curve of the DAHL method gradually deviates from the CRLB, but it still has better estimation accuracy than the DAHL without AOA method. The reason for this is that although the AOA measurement value does not include the velocity information of the mobile node, the azimuth and elevation measurement information obtained by DAHL during the localization process can provide additional information for the velocity estimation. The measurement data of the AOA composed of

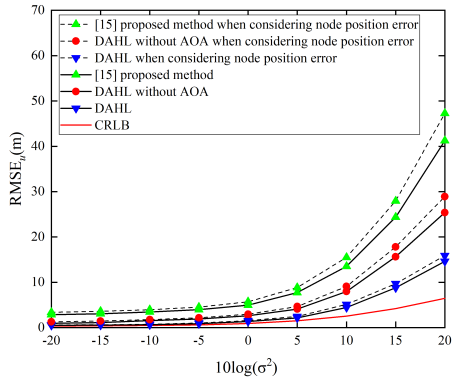

FIGURE 7. The RMSE of the mobile node position estimation when σ_f and σ_{AOA} change at the same time.

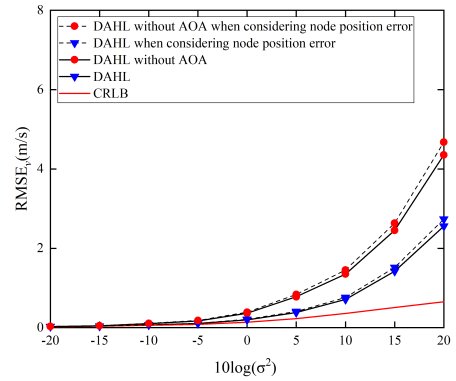

FIGURE 8. The RMSE of the mobile node velocity estimation when σ_f and σ_{AOA} change at the same time.

azimuth and elevation constitute the equation that restricts the velocity estimation in two stages.

Fig. 7 and Fig. 8 show the performance of the three algorithms in estimating the position and velocity, respectively, of the node when the changes in Doppler shift and AOA measurement error level are considered. In the simulation, the following equivalent relations are set: $\sigma_f = \sigma$ and $\sigma_\alpha = \sigma_\beta = 0.2\sigma$. Since σ_f and σ_{AOA} are changed at the same time in the simulation, and Fig. 7 and Fig. 8 show that with the increase in σ_f and σ_{AOA}, the position estimation error and velocity estimation error of the three algorithms also increase, which is the expected result.

In the actual ocean environment, a huge challenge for the position of anchor nodes and ordinary nodes in UWSNs is the ocean currents. Although the anchor nodes and ordinary nodes in the scenario set in this article are connected to the shore-based by cables, these nodes will drift in a small range with ocean currents and cause position deviations.

When the deployed nodes have position errors, to verify the adaptability of the DAHL algorithm, it is assumed that the position deviation of anchor nodes and ordinary nodes in the x, y, and z directions is 5 m, and the position error obeys Gaussian distribution. In the simulation, based on the real position of the deployed node, and 5 m as the standard deviation, randomly generated the position coordinates of nodes with errors. Other parameters are the same as the settings under the condition of no position errors. The dotted lines in Fig. 7 and Fig. 8 show the accuracy of different algorithms for estimating the position and velocity of the mobile node when there are position errors in both anchor nodes and ordinary nodes.

Fig. 7 is demonstrated that the overall accuracy of the DAHL method is better than that of the method proposed in [15] and the DAHL without AOA method, which shows that the localization method combined with Doppler shift and AOA measurement can efficiently improve the localization accuracy of the mobile node. When the Doppler shift and the AOA measurement error are small, the localization accuracy of the DAHL method for the mobile node is extremely close to the CRLB. With the increase in σ, the localization estimation accuracy of the three methods for the mobile node gradually decreases. When the measurement error is large, compared with the DAHL without AOA method and the method proposed in [15], the localization accuracy of DAHL is significantly enhanced. The reason for the poor localization accuracy of the method in [15] is that it does not fully consider the motion characteristics of the mobile node. However, DAHL without AOA uses only a single measurement parameter to locate the mobile node, and its localization accuracy is significantly reduced compared with the DAHL method that uses two measurement parameters.

As shown in Fig. 8, when the DAHL without AOA method is $\sigma = 0.316$, the RMSE$_v$ of the mobile node starts to deviate from the CRLB. When $\sigma < 0.562$, the RMSE$_v$ estimated by the DAHL algorithm for the velocity of the mobile node can basically reach the CRLB. It can be seen from Fig. 8 that as σ increases, the degree of deviation in the RMSE$_v$ from the CRLB gradually increases. The velocity estimation performance of the DAHL method and DAHL without AOA method gradually decreases; however, compared with the DAHL without AOA method, the DAHL estimates the velocity of the mobile node to be closer to the CRLB. It shows that when the Doppler shift measurement is utilized to estimate the motion information of the mobile node, the addition of the AOA measurement helps to improve the position and velocity estimation performance, causing the DAHL method to be more robust than other algorithms. Due to anchor nodes and ordinary nodes in the UWSN are anchored to the seabed by chains, although ocean currents and tides may cause the nodes to drift, the range of their free drift is limited to a fixed area. For the DAHL algorithm, it can be seen from the changes in the RMSE curves in Fig. 7 and Fig. 8 that the position error of anchor nodes and ordinary nodes has a minor effect on the localization accuracy of the mobile node.

2) The LOCALIZATION ACCURACY OF THE ALGORITHM UNDER DIFFERENT TRANSMISSION RANGE CONDITIONS

Taking into account the practicality of the DAHL in the ocean, and at the same time, to consider the localization performance of the DAHL when the number of anchor nodes and the

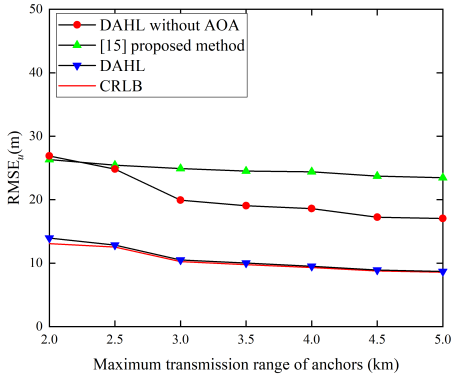

FIGURE 9. The RMSE of the mobile node position estimation when the maximum transmission range of anchor nodes changes.

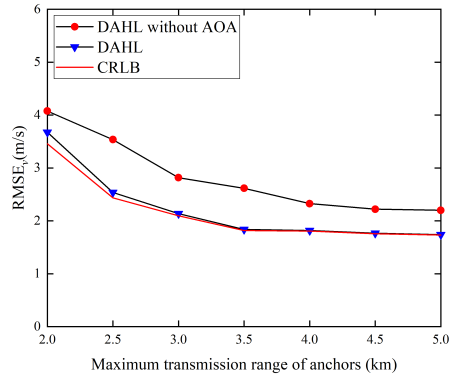

FIGURE 10. The RMSE of the mobile node velocity estimation when the maximum transmission range of anchor nodes changes.

maximum transmission range variation in a 3D underwater scene, the deployment area of the UWSN is expanded to 4000 m × 4000 m × 400 m. In this area, at a depth of 400m, there are 9 anchor nodes are evenly arranged at 2 km intervals. And the carrier frequency of the signal transmitted by the anchor node is selected in turn from 10 kHz to 18 kHz. The transmission range of the anchor node can be changed by adjusting its transmitting power. In the simulation, the transmission range of the anchor node is changed to verify the localization effect of the DAHL algorithm. It is assumed that the Doppler shift measurement error deviation is constant at 2 Hz and the AOA measurement error deviation is constant at 1 deg. The position parameters of the mobile node and the ordinary nodes with no modification. Fig. 9 and Fig. 10 respectively show that when the transmission range of the anchor node changes, the RMSE of the mobile node position estimation and the RMSE of the velocity estimation.

It can be seen from Fig. 9 and Fig. 10 that when the transmission range of anchor nodes gradually increases from 2 km to 5 km, the position estimation accuracy and velocity estimation accuracy of the mobile node are gradually growing. This is because the increase in the transmission range means that more anchor nodes are used by the DAHL algorithm. In the process of locating the mobile node, ordinary nodes need to use the monitoring signal transmitted by anchor nodes and the reflected signal from the mobile node to measure the Doppler shift and AOA. More anchor nodes can enable ordinary nodes to obtain more measurement data containing the position and velocity information of the mobile node, thereby further improving the localization performance of the DAHL. When the transmission range reaches 5 km, the anchor nodes deployed in the area of 4000 m × 4000 m × 400 m will all participate in the localization process. At this time, the localization accuracy of the DAHL is optimal.

Although the transmission range of anchor nodes increases (the number of anchor nodes involved in localization increases) to obtain more measurement data, the cost of deploying a single anchor node in the actual ocean environment is about hundreds of thousands, and the substantial increase in anchor nodes will inevitably greatly surge the cost of the system. Therefore, subject to environmental challenges and deployment costs, it is necessary to ensure a moderate number of nodes and a relatively sparse distribution on the premise that the transmission range of the anchor node can completely cover the entire monitoring area.

In summary, from the above simulation results, compared with the method for locating a stationary node and of the method for locating a mobile node using only single measurement information, the DAHL algorithm proposed in this article demonstrates high localization accuracy and superiority in the localization process.

VII. CONCLUSION

In this article, a hybrid localization algorithm based on Doppler shift and AOA measurements is proposed. The method aims to provide a solution for locating the mobile node in a 3D UWSN. Through comprehensive analysis of the Doppler shift and AOA measurement data obtained by ordinary nodes, auxiliary parameters are introduced to transform the nonlinear equation formed by the Doppler shift and AOA measurement values into a pseudolinear equation, and then the localization information of the mobile node are estimated. Finally, the accurate estimation values of the position and velocity can be further obtained by optimizing the estimation error. Theoretical and simulation experiments show that for a mobile node, DAHL can reliably estimate its instantaneous position and velocity in the simulation under the condition of small measurement error. When the measurement error increases, the method has shown high performance in estimating the position and velocity. After the mobile node is accurately located and its velocity has been obtained, it can be monitored and tracked in real time. In future work, a tracking algorithm for the mobile node will be further designed on the basis of the DAHL algorithm to improve the monitoring, defense, and control capabilities of UWSNs in the deployment area.

REFERENCES

[1] G. Tuna and V. C. Gungor, "A survey on deployment techniques, localization algorithms, and research challenges for underwater acoustic sensor networks," *Int. J. Commun. Syst.*, vol. 30, no. 17, Nov. 2017, Art. no. e3350.

[2] K. Hao, H. Shen, Y. Liu, B. Wang, and X. Du, "Integrating localization and energy-awareness: A novel geographic routing protocol for underwater wireless sensor networks," *Mobile Netw. Appl.*, vol. 23, no. 5, pp. 1427–1435, Oct. 2018.
[3] N. Saeed, A. Celik, T. Y. Al-Naffouri, and M. S. Alouini, "Underwater Optical Wireless Communications, Networking, and Localization: A Survey," *Ad Hoc Netw.*, vol. 94, Nov. 2019, Art. no. 101935.
[4] Q. Fengzhong, W. Shiyuan, W. Zhihui, and L. Zubin, "A survey of ranging algorithms and localization schemes in underwater acoustic sensor network," *China Commun.*, vol. 13, no. 3, pp. 66–81, Mar. 2016.
[5] M. Erol-Kantarci, H. T. Mouftah, and S. Oktug, "A survey of architectures and localization techniques for underwater acoustic sensor networks," *IEEE Commun. Surveys Tuts.*, vol. 13, no. 3, pp. 487–502, 3rd Quart., 2011.
[6] S. Zhao, B. M. Chen, and T. H. Lee, "Optimal sensor placement for target localisation and tracking in 2D and 3D," *Int. J. Control*, vol. 86, no. 10, pp. 1687–1704, Oct. 2013.
[7] Z. Gong, C. Li, and F. Jiang, "Passive underwater event and object detection based on time difference of arrival," in *Proc. IEEE Global Commun. Conf. (GLOBECOM)*, Dec. 2019, pp. 1–6.
[8] K. Hao, K. Yu, Z. Gong, X. Du, Y. Liu, and L. Zhao, "An enhanced AUV-aided TDoA localization algorithm for underwater acoustic sensor networks," *Mobile Netw. Appl.*, early access, Jun. 6, 2020, doi: 10.1007/s11036-020-01577-5.
[9] S. Poursheikhali and H. Zamiri-Jafarian, "Received signal strength based localization in inhomogeneous underwater medium," *Signal Process.*, vol. 154, pp. 45–56, Jan. 2019.
[10] H. Huang and Y. R. Zheng, "Node localization with AoA assistance in multi-hop underwater sensor networks," *Ad Hoc Netw.*, vol. 78, pp. 32–41, Sep. 2018.
[11] Y. Sun, Y. Yuan, Q. Xu, C. Hua, and X. Guan, "A mobile anchor node assisted RSSI localization scheme in underwater wireless sensor networks," *Sensors*, vol. 19, no. 20, p. 4369, Oct. 2019.
[12] L. E. Emokpae and M. Younis, "Throughput analysis for shallow water communication utilizing directional antennas," *IEEE J. Sel. Areas Commun.*, vol. 30, no. 5, pp. 1006–1018, Jun. 2012.
[13] I. Ullah, J. Chen, X. Su, C. Esposito, and C. Choi, "Localization and detection of targets in underwater wireless sensor using distance and angle based algorithms," *IEEE Access*, vol. 7, pp. 45693–45704, 2019.
[14] L. E. Emokpae, S. DiBenedetto, B. Potteiger, and M. Younis, "UREAL: Underwater reflection-enabled acoustic-based localization," *IEEE Sensors J.*, vol. 14, no. 11, pp. 3915–3925, Nov. 2014.
[15] L. Rui and K. Ho, "Efficient closed-form estimators for multistatic sonar localization," *IEEE Trans. Aerosp. Electron. Syst.*, vol. 51, no. 1, pp. 600–614, Jan. 2015.
[16] T. Jia, H. Wang, X. Shen, Z. Jiang, and K. He, "Target localization based on structured total least squares with hybrid TDOA-AOA measurements," *Signal Process.*, vol. 143, pp. 211–221, Feb. 2018.
[17] C. Zheng, D. Sun, L. Cai, and X. Li, "Mobile node localization in underwater wireless networks," *IEEE Access*, vol. 6, pp. 17232–17244, 2018.
[18] P. A. M. de Theije and J.-C. Sindt, "Single-ping target speed and course estimation using a bistatic sonar," *IEEE J. Ocean. Eng.*, vol. 31, no. 1, pp. 236–243, Jan. 2006.
[19] R. Diamant, L. M. Wolff, and L. Lampe, "Location tracking of ocean-current-related underwater drifting nodes using Doppler shift measurements," *IEEE J. Ocean. Eng.*, vol. 40, no. 4, pp. 887–902, Oct. 2015.
[20] K. Papakonstantinou and D. Slock, "Hybrid TOA/AOD/Doppler-shift localization algorithm for NLOS environments," in *Proc. IEEE 20th Int. Symp. Pers., Indoor Mobile Radio Commun.*, Sep. 2009, pp. 1948–1952.
[21] P. Carroll, K. Domrese, H. Zhou, S. Zhou, and P. Willett, "Doppler-aided localization of mobile nodes in an underwater distributed antenna system," *Phys. Commun.*, vol. 18, pp. 49–59, Mar. 2016.
[22] Y. Kalkan and B. Baykal, "Frequency-based target localization methods for widely separated MIMO radar," *Radio Sci.*, vol. 49, no. 1, pp. 53–67, Jan. 2014.
[23] Z. Gong, C. Li, and F. Jiang, "Analysis of the underwater multi-path reflections on Doppler shift estimation," *IEEE Wireless Commun. Lett.*, early access, Jun. 19, 2020, doi: 10.1109/LWC.2020.3003743.
[24] Z. Gong, C. Li, F. Jiang, and J. Zheng, "AUV-aided localization of underwater acoustic devices based on Doppler shift measurements," *IEEE Trans. Wireless Commun.*, vol. 19, no. 4, pp. 2226–2239, Apr. 2020.
[25] J. Wang, Z. Qin, Y. Bi, S. Wei, and F. Luo, "Target localisation in multistatic radar using BR, TDOA, and AOA measurements," *J. Eng.*, vol. 2019, no. 19, pp. 6052–6056, Oct. 2019.
[26] H. W. Sorenson, *Parameter Estimation: Principles and Problems*, vol. 9. New York, NY, USA: M. Dekker, 1980.
[27] S. M. Kay, *Fundamentals of Statistical Signal Processing*. Upper Saddle River, NJ, USA: Prentice-Hall, 1993.

KUN HAO received the M.S. degree from Tianjin University, Tianjin, China, in 2006, and the Ph.D. degree from the School of Computer Science and Technology, Tianjin University, in 2010. She is currently an Associate Professor with the School of Computer and Information Engineering, Tianjin Chengjian University. Her research interests include underwater sensors networks, wireless communications and networking, wireless sensor networks, network protocol and network optimization, and application of VR technology in architecture design.

QIXIN XUE is currently pursuing the M.S. degree in computer science and technology with Tianjin Chengjian University, Tianjin, China. From 2018 to 2020, he was a Student with the Underwater Communication Group, Tianjin Chengjian University. His research interests include wireless communications and networking, the development of underwater sensors networks, underwater senor networks localization, and underwater acoustic localization.

CHENG LI (Senior Member, IEEE) received the B.Eng. and M.Eng. degrees from the Harbin Institute of Technology, Harbin, China, in 1992 and 1995, respectively, and the Ph.D. degree in electrical and computer engineering from Memorial University, St. John's, NL, Canada, in 2004. He is currently a Full Professor with the Department of Electrical and Computer Engineering, Faculty of Engineering and Applied Science, Memorial University. His research interests include mobile ad hoc and wireless sensor networks, wireless communications and mobile computing, switching and routing, and broadband communication networks. He is a Registered Professional Engineer in Canada and a Senior Member of the IEEE Communications Society, the IEEE Computer Society, the IEEE Ocean Engineering Society, and the IEEE Vehicular Technology Society.

KAICHENG YU is currently pursuing the M.S. degree in computer science and technology with Tianjin Chengjian University, Tianjin, China. From 2017 to 2018, he was a Student with the Underwater Communication Group, Tianjin Chengjian University. His research interests include the development of underwater sensors networks, wireless communications and networking, wireless sensor networks, network protocol, and network optimization.